Analytical solution for coupled water–gas transport in landfill cover

He-Fu Pu[1] · Xiao-Jun Wen[1] · Ming Min[1] · Jiannan Chen[2] · Jin-Wei Qiu[3]

Abstract
The transport of water and gas is the most important process for the performance evaluation of landfill cover. However, the transport behaviors of these two components have been calculated separately (i.e., ignoring their coupling effect) in analytical solutions due to the complexity, although this coupling effect has been widely demonstrated in numerical studies, laboratory tests, and field tests. This study presents an analytical solution for coupled water–gas transport in a single-layer landfill cover, which can consider transient diffusive–advective transport of gas under steady-state water transport. The proposed analytical solution is verified against the field data, laboratory data, and numerical simulations. Parametric study is conducted to investigate the effects of four important parameters (i.e., infiltration rate, evaporation rate, desaturation coefficient, and saturated coefficient of water permeability) on the coupled water–gas transport behaviors, and the results indicate that these parameters all have a significant impact on the coupled water–gas transport (e.g., the gas emission flux for the case with desaturation coefficient $\alpha = 0.9$ m^{-1} is 11.9 times greater than that with $\alpha = 0.3$ m^{-1}). For the simulations considered, ignoring the coupling effect would underestimate the steady-state gas emission flux by about 10.9–54.2%, due to the changes of gas transport properties induced by water transport. The magnitude of this underestimation (i.e., error induced by ignoring the coupling effect) increases with decreasing infiltration rate, increasing evaporation rate, increasing desaturation coefficient, and decreasing saturated coefficient of water permeability.

1 Introduction

The safe disposal of waste materials (e.g., municipal solid waste (MSW) and industrial solid waste) is a global issue due to their huge volume and continuous increase. At present, landfilling is still the most common method for solid waste disposal due to its relatively low cost

✉ Ming Min
  jakemin@126.com

✉ Jiannan Chen
  jiannan.chen@ucf.edu

[1] School of Civil and Hydraulic Engineering, Huazhong University of Science and Technology, Wuhan 430074, Hubei, China

[2] Department of Civil, Environmental, and Construction Engineering, University of Central Florida, Orlando, FL 32816, USA

[3] Key Laboratory of Geotechnical Mechanics and Engineering of the Ministry of Water Resources, Changjiang River Scientific Research Institute, Wuhan 430010, Hubei, China

[2, 24, 26]. The final cover system is required for the landfill closure to prevent the gas migration into and/or out of the wastes and to reduce the leachate generation, greenhouse gas emission, and landfill odor [15, 29].

Prediction of the transport processes of water and gas is important for the design and performance evaluation of cover system. Many researchers have presented analytical solutions for predicting the transport of water and gas in soils. However, the analytical solutions for water transport neglect the effect of gas transport [10, 19, 21, 36, 39], whereas those for gas transport neglect the effect of water transport [7, 17, 31, 34]. In reality, however, it has been well illustrated by field studies [41] and laboratory studies [40, 42] that the water transport process and the gas transport process mutually influence each other. For example, Zhan et al. conducted a soil column test to study the coupled water and gas transport in a loess cover, and indicated that the increasing volumetric water content (from 0.36 to 0.49) caused by rainfall infiltration reduced the coefficient of gas permeability of the compacted loess by 98% (from 3.67×10^{-12} to 5.73×10^{-14} m^2). This

coupling effect needs to be accounted for if one desires a more accurate analysis of the water–gas transport through the cover system. To the authors' knowledge, all the analytical solutions in the literature have treated the transport of water and that of gas separately, and no analytical solution has been proposed to predict the coupled water–gas transport, although this coupling effect has been investigated by numerical simulations [6, 16, 18]. Compared with numerical methods, the analytical solutions are frequently preferred because they have clear mathematical expression and thus provide more straightforward understanding of the mechanisms behind the gas/water transport behaviors [33]. Furthermore, the analytical solutions have better numerical stability and higher computational speed than the numerical methods [5].

In this paper, analytical solution is proposed for predicting the coupled water–gas transport in a single-layer unsaturated cover. The novelty of the proposed analytical solution is that the transient diffusive-advective gas transport can be considered by taking into account the effect of water flow in the cover soil rather than simply assuming a constant water content distribution as is the case in the available analytical solutions. It's worth mentioning that the solution proposed in the present study only accounts for the influence of water transport on gas transport and not the other way around. In other words, the proposed solution is a semi-coupled solution, rather than a fully-coupled solution. The gas transport analysis in this study is in the period after the water flow has reached steady state after the rainfall and/or evaporation. The proposed analytical solution is verified by comparing with the existing field test, laboratory test from the literature and numerical simulations. Parametric study is conducted to investigate the effects of four important parameters (i.e., infiltration rate, evaporation rate, desaturation coefficient and saturated coefficient of water permeability) on the gas emission flux and pore water pressure distribution in the cover. Importantly, the significance of considering the effect of water–gas coupling is also studied.

2 Mathematical model

Figure 1 shows the schematic of an unsaturated soil cover overlying a waste mound. Rainfall infiltration or evaporation is specified at the top surface of the cover, and the landfill gas generated by the waste moves upward. A coordinate system is established with the vertical coordinate z directed upward from the bottom of the cover, with the thickness of the cover = L.
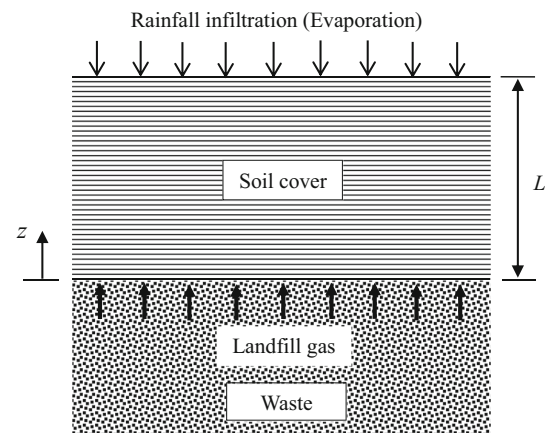

Fig. 1 Configuration of landfill cover with one-dimensional water transport and gas transport

2.1 Water transport

The one-dimensional nonlinear differential equation describing the water transport in unsaturated soils is expressed as follows [27]:

$$\rho_w \frac{\partial \theta_w}{\partial t} = \frac{\partial}{\partial z}\left[\rho_w k(h) \frac{\partial}{\partial z}(h+z)\right] \tag{1}$$

where ρ_w is the water density; h is the pressure head; θ_w is the volumetric water content; k is the coefficient of water permeability for unsaturated soils; t is the time; and z is the elevation in the vertical direction.

According to Gardner [8], the coefficient of water permeability and volumetric water content are assumed to be functions of pore water head h, and can be expressed as follows:

$$\begin{cases} k(h) = k_s e^{\alpha h} \\ \theta(h) = \theta_r + (\theta_s - \theta_r)e^{\alpha h} \end{cases} \tag{2}$$

where θ_s is the saturated volumetric water content; θ_r is the residual volumetric water content; k_s is the saturated coefficient of water permeability of the soil; and α is the desaturation coefficient and is related to the soil's pore size distribution.

The analytical solution [10] for steady-state water transport in an unsaturated single-layer soil cover with infiltration or evaporation surface boundaries can be expressed as:

$$h = \frac{1}{\alpha}\ln(c_1 e^{-\alpha z} + c_2) \tag{3}$$

where c_1 and c_2 are nonzero coefficients that depend on the infiltration and evaporation boundary conditions and can be expressed as:

$$\begin{cases} c_1 = e^{\alpha h_0} - \dfrac{q}{k_s} \\ c_2 = \dfrac{q}{k_s} \end{cases} \tag{4}$$

where q is the infiltration or evaporation rate at the surface of the cover. Two different surface boundaries (i.e., infiltration boundary and evaporation boundary) are considered for the water transport in the cover.

The surface boundary with prescribed flux condition is expressed as:

$$\left[k(h)\frac{\partial h}{\partial z} + k(h) \right]_{z=L} = \begin{cases} q_{01} \ t \le t_p \ (\text{infiltration stage}) \\ q_{02} \ t > t_p \ (\text{evaporation stage}) \end{cases} \tag{5}$$

where q_{01} is the infiltration rate (i.e., rainfall rate, positive value); q_{02} is the evaporation rate (negative value); and t_p is the duration of rainfall. Although the water transport process is assumed to be steady-state, two separate processes of infiltration and evaporation are considered for the surface boundary of the cover to better simulate the actual situation, that is, the infiltration stage (before t_p) and the evaporation stage (after t_p) correspond to two different steady states of water distribution in the cover.

The surface boundary with constant pressure head condition is expressed as:

$$h(z,t)|_{z=L} = h_1 \tag{6}$$

The bottom boundary condition is expressed as:

$$h(z,t)|_{z=0} = h_0 \tag{7}$$

Initial condition is expressed as:

$$h(z,t)|_{t=0} = h_i(z) \tag{8}$$

2.2 Gas transport

Several assumptions are adopted to simply the gas transport: (i) the diffusion and advection of gas transport in the cover system are considered transient (i.e., change with time) and one-dimensional; (ii) temperature is assumed constant; and (iii) gas flow will not affect the water transport. The governing equation for landfill gas transport through the unsaturated cover can be expressed as [14]:

$$\frac{\partial}{\partial t}\left(\theta_g C_g + \theta_w C_w\right) = \frac{\partial F}{\partial z} - \frac{\partial\left(v_w C_w + v_g C_g\right)}{\partial z} - \mu\theta_g C_g \tag{9}$$

where C_g is the molar concentration of landfill gas; C_w ($= H_g C_g$) [25] is the molar concentration of gas dissolved in water, and H_g is the Henry's coefficient; θ_g and θ_w are the volumetric gas content and volumetric water content, respectively; v_w is the velocity of water flow; v_g is the advective velocity of gas; μ is the degradation rate of gas

[34]; and F is the diffusive flux of gas in gaseous phase and can be expressed as:

$$F = \theta_g D_s \frac{\partial C_g}{\partial z} \tag{10}$$

where D_s is the effective diffusion coefficient of gas ($= \tau D_g$), D_g is the molecular diffusion coefficient of gas, and τ is the correction factor which depends on the soil porosity and the length of gas transport path, and is given as follows [12]:

$$\tau = \frac{\left[(1 - S_w)\phi\right]^{10/3}}{\phi^2} \tag{11}$$

where S_w is the degree of water saturation of soil and ϕ is the soil porosity.

According to Darcy's law, v_w can be expressed as (following Huang and Wu [10]):

$$v_w = -k(h)\left(\frac{\partial h}{\partial z} + 1\right) \tag{12}$$

According to Darcy's law, v_g can be expressed as (following Parker [22]):

$$v_g = -k_g \frac{\partial P_g}{\partial z} = -k_{rg}\frac{k_i}{\mu_g}\frac{\partial P_g}{\partial z} \tag{13}$$

where k_g is the coefficient of gas permeability; P_g is the gas pressure and is assumed to change linearly with depth in the soil; k_i is the intrinsic permeability of soil; μ_g is the viscosity of gas; and k_{rg} is the relative coefficient of gas permeability and is given as follows [22]:

$$k_{rg} = \sqrt{1 - S_e}\left[1 - S_e^{1/m}\right]^{2m} \tag{14}$$

where S_e is the effective degree of water saturation of soil and, under isothermal condition, is given as

$$S_e = \frac{\theta - \theta_r}{\theta_s - \theta_r} \tag{15}$$

Two different bottom boundary conditions, i.e., flux boundary and concentration boundary, are considered for gas transport in the cover.

Bottom boundary condition is expressed as:

$$\begin{cases} F_b|_{z=0} = F_0 & \text{if mass flux boundary} \\ C_g(z,t)|_{z=0} = C_b e^{-\lambda t} & \text{if concentration boundary} \end{cases} \tag{16}$$

where C_t is the gas concentration at the cover surface; F_0 is a constant; C_b is the peak gas concentration at the cover bottom; and λ is the first order decay rate. At the initial stage after landfill closure, the gas production from the degradation of waste mass increases with time [3, 30], and this stage can be simplified using a flux boundary; later, as the service life of the landfill increases and the degradation of most wastes is close to completion, the gas

concentration decreases with time and tends to stabilize [1, 30] and, at this stage, this boundary condition can be simplified using a concentration boundary.

Surface boundary condition is expressed as:

$$C_g(z,t)\big|_{z=L} = C_t \tag{17}$$

The initial condition of Eq. (9) can be expressed as follows:

$$C_g(z,t)\big|_{t=0} = g(z) \tag{18}$$

3 Analytical solution

Assume that $C_g(z, t)$ is determined by the following equation:

$$C_g(z,t) = u_g(z,t) + (1 - z/L)B_t + C_t z/L \tag{19}$$

where

$$\begin{cases} \dfrac{F_0}{\theta_g D_s}\bigg|_{z=0} & \text{for flux boundary} \\ C_b e^{-\lambda t} & \text{for concentration boundary} \end{cases} \tag{20}$$

Substituting Eq. (19) into Eq. (9), the governing equation for $u_g(z, t)$ can be obtained as

$$\frac{\partial u_g}{\partial t} = \frac{\theta_g D_s}{\theta_g + \theta_w H_g}\frac{\partial^2 u_g}{\partial z^2} + \frac{\partial(\theta_g D_s)/\partial z - (v_w H_g + v_g)}{\theta_g + \theta_w H_g}\frac{\partial u_g}{\partial z}$$
$$- \frac{\partial(v_w H_g + v_g)/\partial z + \mu\theta_g}{\theta_g + \theta_w H_g}u_g + G(z,t) \tag{21}$$

where

$$G(z,t) = \frac{\partial(\theta_g D_s)/\partial z - (v_w H_g + v_g)}{(\theta_g + \theta_w H_g)L}(C_t - B_t) - \frac{\partial B_t}{\partial t}\left(1 - \frac{z}{L}\right)$$
$$- \frac{\partial(v_w H_g + v_g)/\partial z + \mu\theta_g}{\theta_g + \theta_w H_g}\left[\left(1 - \frac{z}{L}\right)B_t + C_t\frac{z}{L}\right] \tag{22}$$

The boundary conditions for Eq. (21) can be obtained by substituting Eq. (19) into Eqs. (16) and (17):

$$u_g(z,t)\big|_{z=L} = 0 \tag{23}$$

$$\begin{cases} \dfrac{\partial u_g(z,t)}{\partial z}\bigg|_{z=0} = 0 \\ u_g(z,t)\big|_{z=0} = 0 \end{cases} \tag{24}$$

The initial condition can be expressed as:

$$u_g(z,t)\big|_{t=0} = g(z) - (1 - z/L)B_t\big|_{t=0} - C_t z/L \tag{25}$$

A generalized integral transform method is used to solve the transport problem described by Eqs. (21) to (25). A pair

of transformation formulae are required for the integral transform method, i.e., the integral and inverse transforms (see details in Appendix 1).

Finally, the analytical solution to Eq. (9) (i.e., gas transport) is obtained by substituting Eq. (43) into Eq. (19) as follows:

$$C_g(z,t) = \mathbf{Y}^T\left[\exp(-\mathbf{H}t)\mathbf{T}(0) + \int_0^t \exp(-\mathbf{H}(t-\tau))\mathbf{G}d\tau\right] + (1 - z/L)B_t + C_t z/L \tag{26}$$

The gas emission flux at the surface of the cover can be calculated as follows:

$$J = \left[C_g(z,t)\times(v_g + v_w H_g) - \theta_g D_s\frac{\partial C_g(z,t)}{\partial t}\right]\bigg|_{z=L} \tag{27}$$

4 Model verification

To verify the proposed analytical solution, the transport results computed using this solution are compared with the commercial software COMSOL Multiphysics 5.5, the field experimental data of Schuetz et al. [28], and the laboratory test data of Ng et al. [18].

### 4.1 Comparison with numerical simulation of commercial software

A commercial software COMSOL, which has been extensively used in the literature, is used in this section. The governing equations (Eqs. (1) and (9)) were user-defined and then solved in COMSOL. The following parameter values are adopted [4, 20]: cover thickness $L = 1.4$ m, saturated volumetric water content $\theta_s = 0.57$, residual volumetric water content $\theta_r = 0.03$, desaturation coefficient $\alpha = 0.01$ m^{-1}, saturated coefficient of water permeability $k_s = 5.7 \times 10^{-8}$ m/s, initial intrinsic permeability $k_i = 1.03 \times 10^{-16}$ m^2, Van Genuchten's parameter $m = 0.67$, diffusion coefficient of gas $D_g = 2.14 \times 10^{-5}$ m^2/s, viscosity of gas $\mu_g = 1.1 \times 10^{-5}$ Pa·s, and Henry's constant $H_g = 0.032$. For the water transport boundary conditions: the surface boundary is a rainfall infiltration condition with a net infiltration rate of 3.65 mm/d and, after the duration of rainfall ($t_p = 5$ d), it changes to evaporation boundary condition with an evaporation rate of 2.91 mm/d; the bottom boundary is a constant water pressure head with an initial degree of water saturation = 0.7. For the gas transport boundary conditions: constant gas concentration (= 0) is applied at the cover surface; two types of boundary condition at the cover bottom are considered (i.e., constant gas concentration

$C_0 = 4$ mol/m^3, and constant gas flux $F_0 = 500$ mol/ha/d (i.e., molarity/hectare/day)). Oxidation of methane is not considered. As shown in Fig. 2, excellent agreement between the proposed analytical solution and numerical simulations are obtained for the coupled transport results, including gas concentration profiles during the infiltration stage and the evaporation stage for the two bottom boundary conditions (Fig. 2a and b), pore water pressure head profiles at the end of the infiltration stage and that of the evaporation stage (Fig. 2c), and surface gas emission flux versus elapsed time for the two different bottom boundaries (Fig. 2d).

4.2 Comparison with field experimental data

Schuetz et al. [28] measured the surface emission of methane and 37 non-methane organic compounds (NMOCs) at Lapouyade landfill, located near Bordeaux, France. Phase I cells have a final cover system that is composed of 40 cm coarse sand and 80 cm fully-vegetated loam. The parameters of the two soil layers are simplified to a single homogeneous layer using the weighted average method. According to the field test conducted by Zhan et al. [37], the following parameter values are adopted: $\theta_s = 0.496$, $\theta_r = 0.119$, $\alpha = 0.7$ m^{-1}, permeability $k_{s-} = 5.0 \times 10^{-7}$ m/s, $k_i = 4.85 \times 10^{-13}$ m^2, $m = 0.346$, $\mu_{g-} = 0.7 \times 10^{-5}$ Pa·s, $D_g = 9.6 \times 10^{-6}$ m^2/s, $H_g = 0.26$, and initial pore water pressure head $h_0 = -0.7$ m. For the water transport boundary conditions: pore water pressure head is constant at the bottom and is equal to the initial pore water pressure head; the evaporation rate was set zero to simulate the humid climate and the infiltration is not considered here [34]. For the gas transport boundary conditions: gas concentrations at the surface and bottom of the cover are both assumed constant. Fig. 3 shows the benzene and ethylbenzene concentration profiles at steady state, and indicates good agreement between the proposed analytical solution and the experimental data of Schuetz et al. [28]. Some
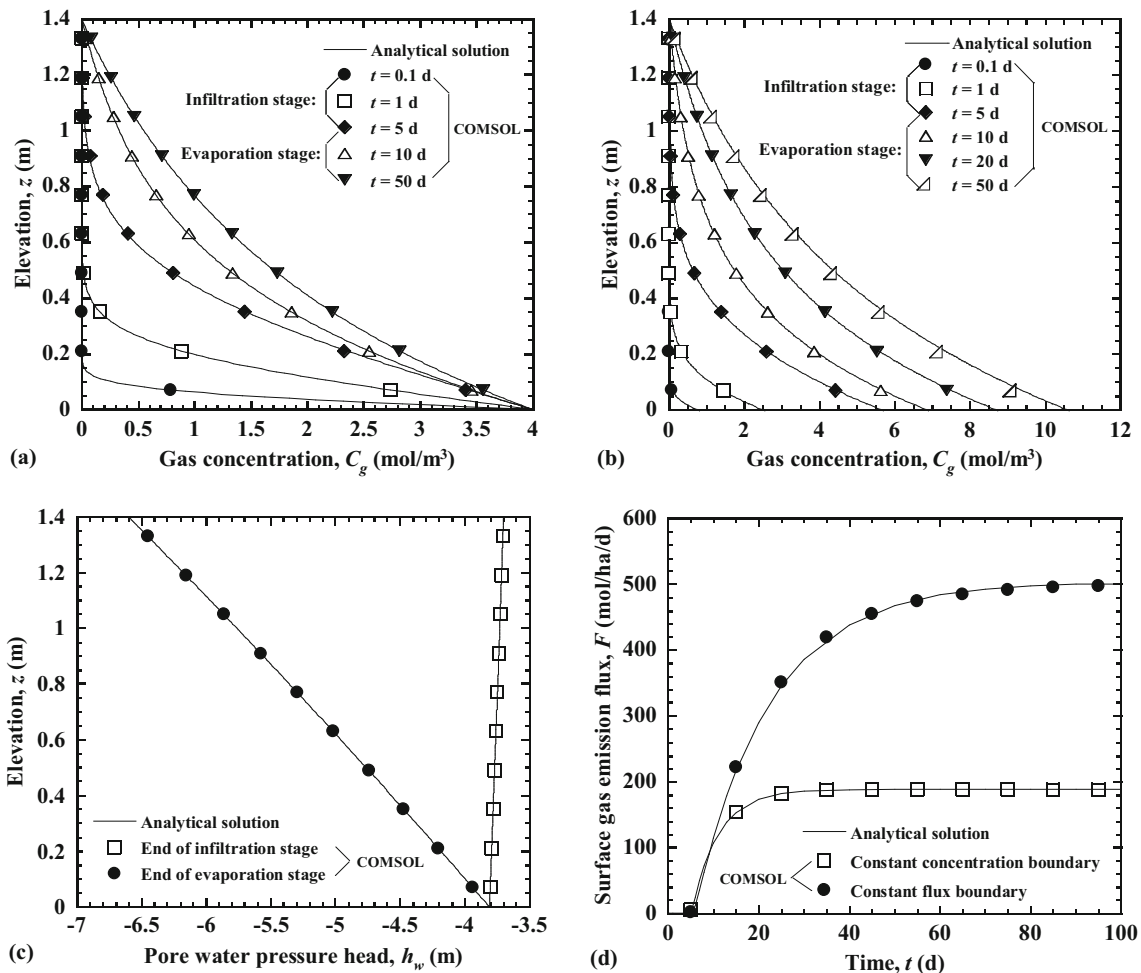
Fig. 2 Comparison of water–gas transport results between analytical solution and the COMSOL simulations: **a** gas concentration profiles for constant concentration bottom boundary; **b** gas concentration profiles for constant flux bottom boundary; **c** pore water pressure head profiles; **d** surface gas emission flux for two different bottom boundaries
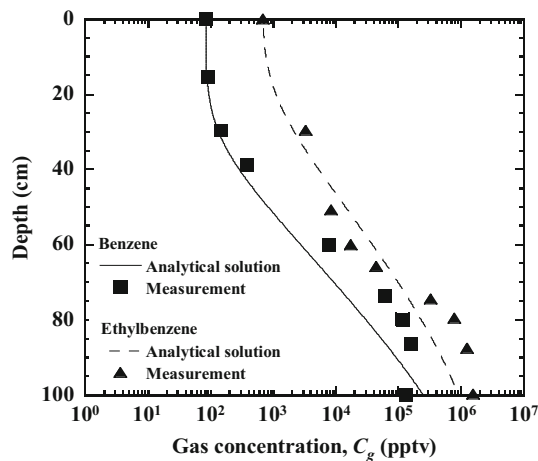
Fig. 3 Comparison of gas concentration profiles at steady state between the proposed analytical solution and the experimental measurement of Schuetz et al. [28]

differences occur at the lower portion of the soil profile probably because the input parameter values (e.g., k_s, θ_s, k_i, and D_g) are assumed constant with depth in the proposed analytical solution, whereas the actual cover system consists of two different soil layers and thus the parameter values vary with depth.

4.3 Comparison with laboratory test data

One-dimensional column tests were conducted on unsaturated compacted clay by Ng et al. [18] to investigate the gas emission flux through landfill cover. For the purpose of verification, the tests at serviceability limit state with low gas pressure ranging from 0 to 20 kPa are chosen, considering the typically low gas pressure (< 10 kPa) generated in landfill. Two different clay thicknesses (i.e., 0.4 m and 0.6 m) and two different degrees of saturation (i.e., 40% and 60%) are chosen. The following parameter values are adopted [4, 18]: $\theta_s = 0.512$, $\theta_r = 0.09$, $\alpha = 1/12$ m^{-1}, $k_s = 5.2 \times 10^{-9}$ m/s, $k_i = 1.2 \times 10^{-15}$ m^2, $m = 0.329$, $D_{g\text{-}} = 2.08 \times 10^{-5}$ m^2/s, $\mu_g = 1.8 \times 10^{-5}$ Pa·s, and $H_{g\text{-}} = 0.016$. For the water transport boundary conditions: constant water pressure head (calculated from the initial degree of saturation) is specified at the bottom boundary, while the evaporation rate is 2 mm/d at the surface boundary. For the gas transport boundary conditions: the surface boundary is connected to the atmosphere and the gas concentration is constant at the bottom. Fig. 4 shows the steady-state gas emission flux at the cover surface as a function of gas pressure at the cover bottom for different values of cover thickness and degree of saturation. Overall, the proposed analytical solution is in good agreement with the laboratory measurement of Ng et al. [18]. Nonetheless, the agreement is not good for the case with S_w of 40% and

low gas pressure (i.e., < 10 kPa) in Fig. 4b, because Eq. (2) is a simplification of the actual soil–water characteristic curve, which will produce a larger deviation when the gas pressure is relatively smaller.

5 Parametric study

To better understand the influencing factors of the water–gas transport in landfill cover, several key parameters (i.e., infiltration rate, evaporation rate, desaturation coefficient and saturated coefficient of water permeability) are investigated using the proposed analytical solution. The cover system is composed of an unsaturated silty clay with a thickness of 1.0 m. The following parameter values are adopted [4, 21, 32]: the saturated volumetric water content $\theta_s = 0.34$, residual volumetric water content $\theta_r = 0.01$, desaturation coefficient $\alpha = 0.13$ m^{-1}, saturated coefficient of water permeability $k_s = 5.0 \times 10^{-7}$ m/s, initial intrinsic permeability $k_i = 1.25 \times 10^{-15}$ m^2, Van Genuchten's parameter $m = 0.115$, viscosity of gas $\mu_g = 1.1 \times 10^{-5}$ Pa·s, diffusion coefficient of gas $D_g = 2.137 \times 10^{-5}$ m^2/s, Henry's constant $H_g = 0.0316$, and initial pore water pressure head $h_0 = -2.0$ m. The cover bottom has a constant gas pressure ($= 5$ kPa) while the cover surface is connected to the atmosphere [18]. For water transport boundary conditions: the infiltration rate = saturated coefficient of water permeability k_s ($= 5.0 \times 10^{-7}$ m/ s = 43.2 mm/d) with a rainfall duration of 5 d, after which the evaporation rate = 2.91 mm/d. For each series of parametric analysis, only the variable of interest was changed, while the other variables remained constant and were equal to the values listed in Table 1, unless otherwise specified. To illustrate the importance of considering the effect of water transport on gas transport, the uncoupled simulation cases that ignored the effect of water transport were also considered, and these cases were conducted using the initial conditions of the cover (e.g., water content, coefficient of permeability and effective gas diffusion coefficient) held constant over the simulation period.

5.1 Effect of infiltration rate

The effect of infiltration rate (i.e., rainfall rate) q_{01} on the transport of water and gas in the cover is investigated using four different q_{01} values ($= 0.5k_s$, $1.0k_s$, $1.5k_s$ and $2.0k_s$, i.e., = 21.6, 43.2, 64.8 and 86.4 mm/d), covering most cases of rainfall rate typically encountered in practice [9, 35]. Fig. 5a presents the steady-state pore water pressure head after the end of rainfall stage for different q_{01}. The negative pore water pressure head decreases with the increase of q_{01} value, because higher infiltration rate leads to greater increases in water content and degree of
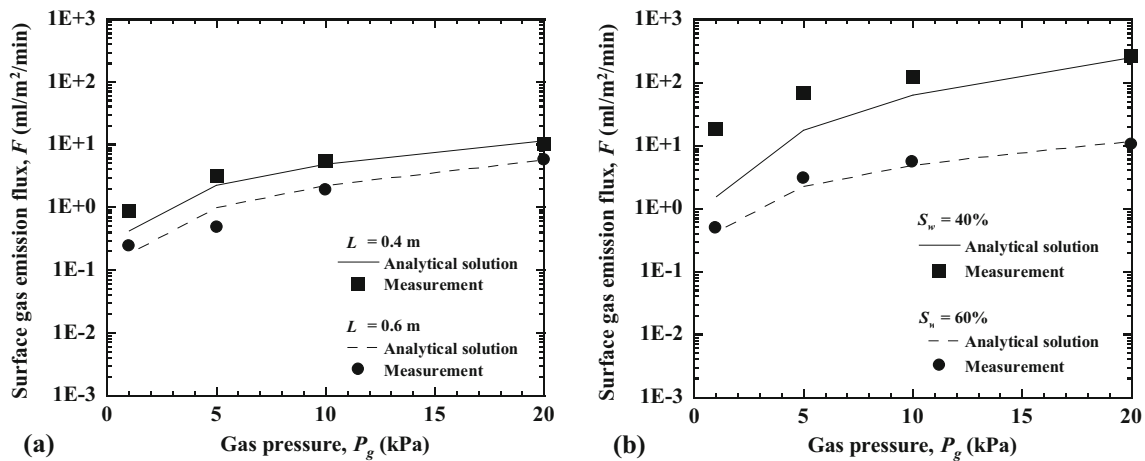
Fig. 4 Comparison of steady-state gas emission flux at the cover surface between the proposed analytical solution and the laboratory measurement of Ng et al. [18]: **a** different cover thickness L, and **b** different degree of water saturation S_w

Table 1 Parameter values used in the parametric study

Parameter	Value	Source
Saturated coefficient of water permeability, k_s (m/s)	5.0×10^{-7}	[32]
Initial intrinsic permeability, k_i (m²)	1.25×10^{-15}	[32]
Saturated volumetric water content, θ_s	0.34	[32]
Residual volumetric water content, θ_r	0.01	[32]
Van Genuchten's parameter, m n	0.115	[32]
Desaturation coefficient, α (m^{-1})	0.13	[32]
Henry's constant, H_g	0.0316	[6]
Diffusion coefficient of gas, D_g (m²/s)	2.137×10^{-5}	[6]
Viscosity of gas, μ_g (Pa·s)	1.1×10^{-5}	[6]
Evaporation rate, q_{02} (mm/d)	2.91	[21]

head in soil (see Eq. (2)). For example, the negative pore water pressure head at the cover surface decreases from –2.34 m to –0.63 m for q_{01} increasing from $0.5k_s$ to $2k_s$. Fig. 5b presents the surface gas emission flux for different q_{01} and indicates that smaller q_{01} value produces earlier gas breakthrough. For example, the gas breakthrough time for $q_{01} = 2k_s$ is about 12 d, which is 71.4% larger than that for $q_{01} = 0.5k_s$ (about 7 d). This is because smaller q_{01} value results in lower water content, higher coefficient of gas permeability and higher effective gas diffusion coefficient (i.e., more pore spaces for gas transport) and thus faster gas transport (e.g., when q_{01} decreases from $2k_s$ to $0.5k_s$, the values of θ_w at the cover surface (calculated using Eq. (2)) after the infiltration stage decrease from 0.314 to 0.254 (19.1% reduction), the corresponding k_g values (calculated
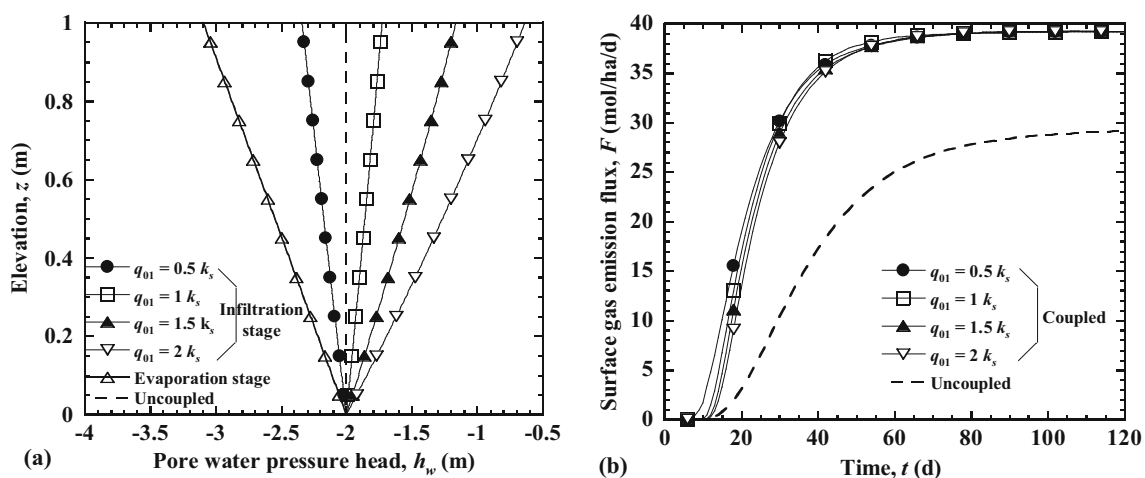
Fig. 5 Effect of infiltration rate q_{01} on coupled water–gas transport in cover: **a** steady-state pore water pressure head; **b** surface gas emission flux

saturation, thus lowering the negative pore water pressure

using Eq. (13)) increase from 2.74 to 5.72×10^{-11} m³·s/kg

(108.8% increase) and the corresponding D_s values (calculated using Eq. (11)) increase from 9.77 to 5.28 × 10^{-8} m^2/s (53 times increase)). In addition, the final, steady-state surface gas emission fluxes for all q_{01} values are the same, because the infiltrated water in the rainfall stage is released in the subsequent evaporation stage and thus all q_{01} values eventually give the same final water content and same coefficient of gas permeability. Fig. 5b also indicates that the maximum gas emission flux for the uncoupled case (= 29.3 mol/ha/d) is only 74.7% (25.3% underestimation) that for the coupled cases (all = 39.2 mol/ha/d), indicating that considering the effect of water transport on gas transport is important.
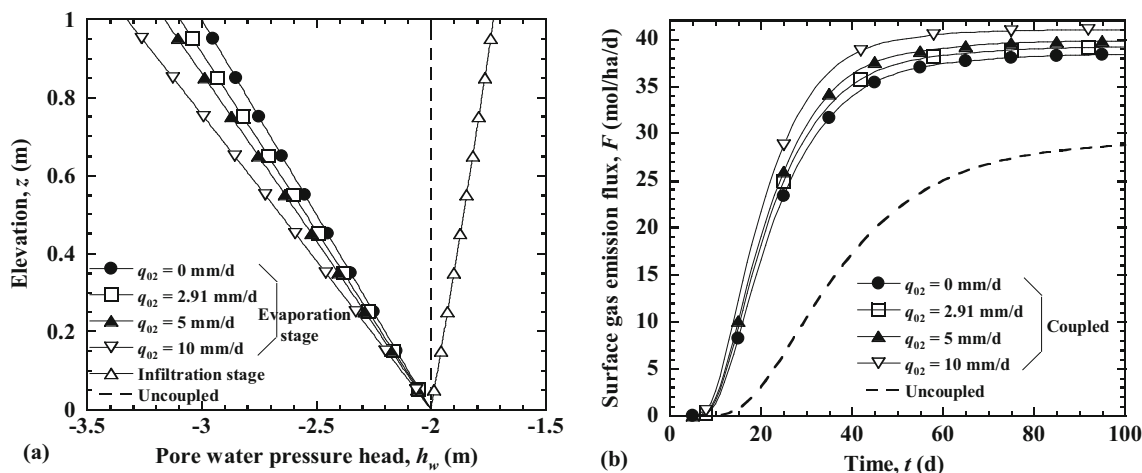
5.2 Effect of evaporation rate

To investigate the effect of evaporation rate q_{02} on the transport of water and gas, four different q_{02} values (= 0, 2.91, 5 and 10 mm/d) are considered using the proposed analytical solution. The q_{02} of zero represents the humid season [11], whereas q_{02} of 5 mm/d and 10 mm/d represent the dry season and extreme dry season. Fig. 6a indicates that the negative pore pressure head increases with increasing evaporation rate. For example, the negative pore water pressure head at the cover surface increases from − 3.00 to − 3.33 m (11.0% decrease) when q_{02} increases from 0 to 10 mm/d. This is because higher evaporation rate produces greater decrease of water content and thus greater suction in soil. Fig. 6b indicates that the surface gas emission flux increases with increasing evaporation rate. For example, the maximum surface gas emission flux increases from 38.4 to 41.1 mol/ha/d (7% increase) when q_{02} increases from 0 to 10 mm/d. This is because higher evaporation rate produces lower water content, higher coefficient of gas permeability and higher effective gas

diffusion coefficient (e.g., when q_{02} increases from 0 to 10 mm/d, the values of θ_w at the cover surface after the evaporation stage decrease from 0.233 to 0.224 (3.9% decrease), the corresponding k_g values increase from 6.41 × 10^{-11} to 6.70 × 10^{-11} m^3·s/kg (4.5% increase) and the corresponding D_s values increase from 1.06 × 10^{-7} to 1.40 × 10^{-7} m^2/s (32.1% increase)), and thus leads to a larger steady-state surface emission flux. Fig. 6b also indicates that the maximum surface gas emission flux for the uncoupled case (= 29.4 mol/ha/d) is much smaller than that for the coupled cases, e.g., is only 71.5% (28.5% underestimation) that for the coupled cases with q_{02} of 10 mm/d (= 41.1 mol/ha/d). This indicates that ignoring the coupling effect would lead to unconservative gas transport result and thus it's important to consider the effect of water transport on gas transport, especially when the evaporation rate is high.
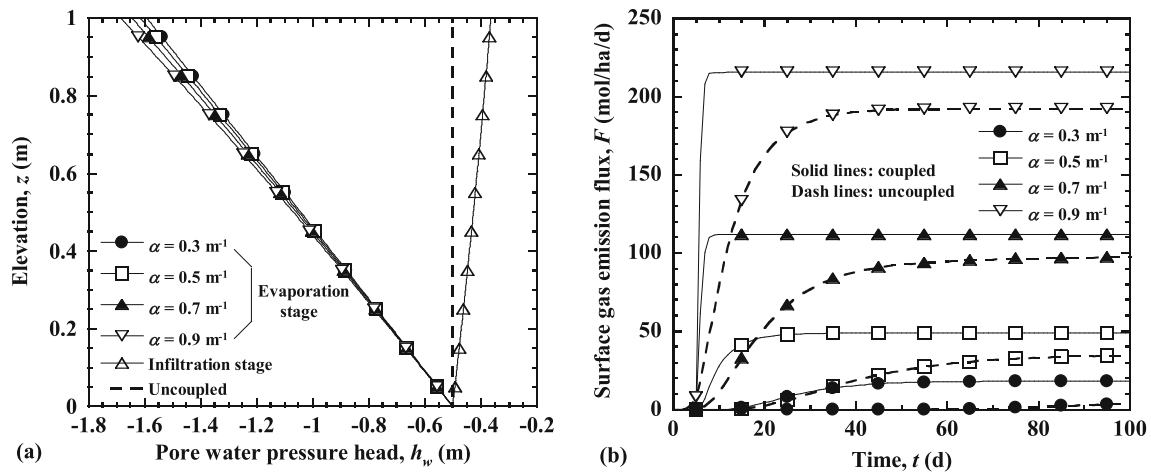
5.3 Effect of desaturation coefficient

The desaturation coefficient α depends on the soil particle size (e.g., finer-grained soil exhibits smaller α) and represents the rate at which the soil water content decreases with increasing matric suction. Previous studies found that the α varies from 0.2 to 5 m^{-1} for most soils [23], and ranges from 0.1 to 1 m^{-1} for most clayey soils that are typically used for landfill cover. Here, four values of α (= 0.3, 0.5, 0.7 and 0.9 m^{-1}) are selected to investigate the effect of desaturation coefficient on the transport of water and gas. Fig. 7a indicates that the negative pore pressure head increases with increasing desaturation coefficient, but the change is slight. For example, when α increases from 0.3 to 0.9 m^{-1}, the pore water pressure head at the cover surface changes from − 1.59 to − 1.69 m. This is because an unsaturated soil with larger soil particle size (larger α) is

Fig. 6 Effect of evaporation rate q_{02} on coupled water–gas transport in cover: **a** steady-state pore water pressure head; **b** surface gas emission flux
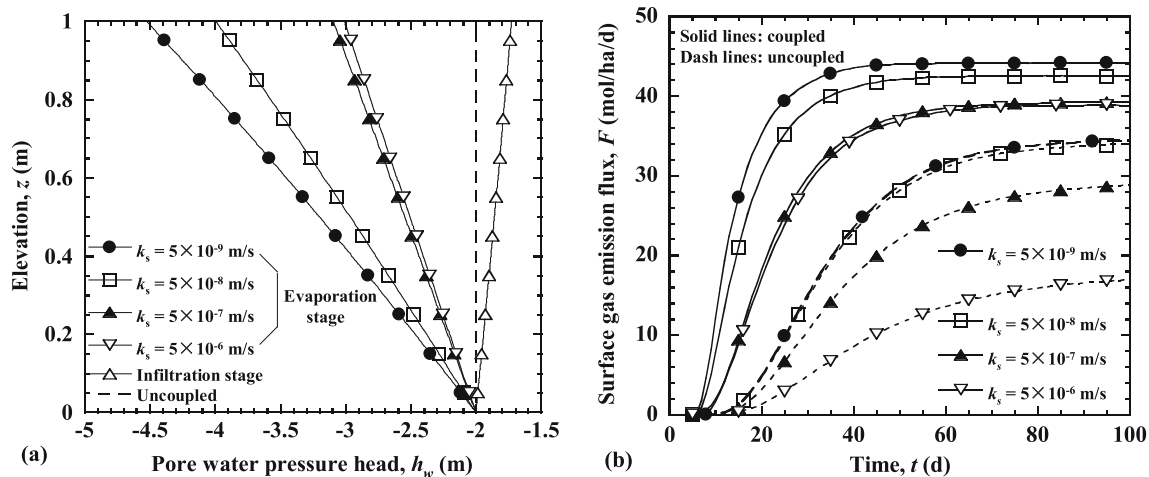
Fig. 7 Effect of desaturation coefficient α on coupled water–gas transport in cover: **a** steady-state pore water pressure head; **b** surface gas emission flux

less inclined to retain water and therefore has a higher negative pore water pressure head at steady state. Fig. 7b indicates that the surface gas emission flux increases significantly with increasing desaturation coefficient. For example, the steady-state gas emission flux increases from 18.1 to 215.7 mol/ha/d (10.9 times increase) when α increases from 0.3 to 0.9 m^{-1}. The time needed for gas transport to reach steady state also changes significantly (e.g., = approximately 16 d and 88 d for α = 0.9 m^{-1} and 0.3 m^{-1}, respectively). This is because, the soil with larger particle size (i.e., larger α) has larger gas-phase pore spaces and thus has higher effective gas diffusion coefficient and faster gas transport (e.g., when α increases from 0.3 to 0.9 m^{-1}, the values of θ_w at the cover surface after the evaporation stage decrease from 0.215 to 0.082 (61.9% reduction), the corresponding k_g values increase from 6.98×10^{-11} to 1.00×10^{-10} m^3·s/kg (43.3% increase) and the corresponding D_s values increase from 1.82×10^{-8} to 2.01×10^{-6} m^2/s (109.4 times increase)). Fig. 7b also indicates that the relative difference between the coupled and uncoupled cases decreases with increasing α value. For example, for α = 0.3 m^{-1}, the maximum gas emission flux for the uncoupled case (= 8.5 mol/ha/d) is only 47.0% (53.0% underestimation) that for the corresponding coupled case (= 18.1 mol/ha/d), while for α = 0.9 m^{-1}, the maximum gas emission flux for the uncoupled case (= 192.2 mol/ha/d) is 89.1% (10.9% underestimation) that for the corresponding coupled case (= 215.7 mol/ha/d). This indicates that considering the effect of water transport on gas transport is important, especially for soils with a small α (i.e., fine-grained soil), because smaller α leads to higher degree of water saturation of cover soil (see Eq. (2))

and, in this case, the soil is more inclined to lose water under evaporation.

5.4 Effect of saturated coefficient of water permeability

The saturated coefficient of water permeability k_s has a significant impact on the water transport process in cover, which in turn changes the coefficient of gas permeability and thus the process of gas transport [38]. To investigate the effect of k_s on the coupled water–gas transport, four different k_s values (= 5×10^{-6}, 5×10^{-7}, 5×10^{-8} and 5×10^{-9} m/s) are considered using the proposed analytical solution. Fig. 8a presents the effect of different k_s on the profiles of pore water pressure head and indicates that smaller k_s produces larger negative pore water pressure head. For example, the negative pore water pressure head at the surface decreases from $-$4.53 m to $-$3.01 m (33.6% reduction) when k_s increases from 5×10^{-9} to 5×10^{-6} m/s. This is because, for soil with smaller k_s, water transport is slower and less water infiltrates into the cover, and thus the soil has lower water content and higher suction. Fig. 8b shows the surface gas emission flux for different k_s values and indicates that the gas emission flux increases with increasing k_s. For example, when k_s increases from 5×10^{-9} to 5×10^{-6} m/s, the maximum gas emission flux decreases from 44.1 to 38.8 mol/ha/d (12.0% decrease), the time needed for gas transport to reach steady state increases from approximately 60 to 90 d (50.0% increase), and the gas breakthrough time increases from approximately 6 to 10 d (66.7% increase). This is because, for a given rainfall rate and evapotranspiration rate, higher k_s value gives a higher water content of soil and correspondingly a lower gas

Fig. 8 Effect of saturated coefficient of water permeability k_s on coupled water–gas transport in cover: **a** steady-state pore water pressure head; **b** surface gas emission flux

permeability and lower effective gas diffusion coefficient (e.g., when k_s increases from 5×10^{-9} to 5×10^{-6} m/s, the values of θ_w at the cover surface after the evaporation stage increase from 0.193 to 0.233 (20.7% increase), the corresponding k_g values decrease from 7.57×10^{-11} to 6.42×10^{-11} m^3·s/kg (15.2% reduction) and the corresponding D_s values decrease from 3.09×10^{-7} to 1.07×10^{-7} m^2/s (65.4% reduction)). Fig. 8b also indicates that the gas emission flux for the uncoupled case is consistently lower than that for the coupled case and the difference increases as the k_s increases. For example, when $k_s = 5 \times 10^{-6}$ m/s, the maximum gas emission flux for the uncoupled case (= 17.8 mol/ha/d) is only 45.8% (54.2% underestimation) that for the coupled case (= 38.9 mol/ha/d). This indicates again that ignoring the coupling effect would lead to unconservative gas transport result and thus it's necessary to consider the effect of water transport on gas transport.

6 Summary and conclusions

This paper presented an analytical solution for coupled water–gas transport in a single-layer landfill cover. The proposed analytical solution was verified by comparing against the laboratory test of Ng et al. [18], the field test of Schuetz et al. [28] and the COMSOL numerical simulations. Using the proposed analytical solution, parametric studies were carried out to investigate the effects of four parameters (i.e., infiltration rate, evaporation rate, desaturation coefficient and saturated coefficient of water permeability) on the surface gas emission flux and pore water

pressure head distribution in the cover. The main conclusions are as follows:

(1) Depending on the conditions (e.g., rainfall rate, evaporation rate, initial conditions, and boundary conditions) and the material properties of soil, the water transport process in the cover can have a significant effect on the gas transport process through the landfill cover. This is because the water transport process changes the distribution of water content inside the cover and thus changes the gas transport properties (e.g., coefficient of gas permeability and effective gas diffusion coefficient).

(2) To illustrate the effect of water transport on the gas transport, two cases of simulations were performed, i.e., coupled case and uncoupled case. The coupled cases considered the effect of water transport on the gas transport. The uncoupled cases ignored the effect of water transport, and were conducted using the initial conditions of the cover (e.g., water content, coefficient of permeability and effective gas diffusion coefficient) held constant over the simulation period. For the simulations considered, the uncoupled cases consistently gave lower transport rate (i.e., unconservative results, e.g., longer gas breakthrough time, and smaller maximum gas emission flux), relative to the coupled cases. Ignoring the coupling effect would underestimate the maximum gas emission flux by about 10.9–54.2%.

(3) The infiltration rate, evaporation rate, desaturation coefficient and saturated coefficient of water permeability all have significant impact on the coupled water–gas transport through the cover. For the simulations considered, the rate of gas transport increases with decreasing infiltration rate, increasing

evaporation rate, increasing desaturation coefficient, and decreasing saturated coefficient of water permeability.

Appendix 1

For our problem, the following eigenvalue system is selected:

$$\frac{d^2\psi_n(z)}{dz^2} + \beta_n^2\psi_n(z) = 0 \tag{28}$$

where β_n is the nth eigenvalue of the system in Eq. (28).

The boundary conditions of the eigensystem in Eq. (28) are

$$\begin{cases} \left.\dfrac{\partial\psi_n(z)}{\partial z}\right|_{z=0} = 0 \\ \left.\psi_n(z)\right|_{z=0} = 0 \end{cases} \tag{29}$$

$$\left.\psi_n(z)\right|_{z=L} = 0 \tag{30}$$

where $\psi_n(z)$ satisfies the following orthogonality relationships:

$$\int_0^L \psi_n(z)\psi_r(z)dz = \begin{cases} 0 & r = n \\ N_n & r \neq n \end{cases} \tag{31}$$

$$N_n = \int_0^L \psi_n^2(z)dz \tag{32}$$

The general solution to the eigenvalue system described by Eqs. (28) to (30) can be expressed as follows:

$$\psi_n(z) = \begin{cases} \cos\left[\dfrac{(2k+1)\pi}{2L}z\right] \\ \sin\left(\dfrac{k\pi}{L}z\right) \end{cases} \tag{33}$$

The pair integral transform can be constructed as:

$$T_n(t) = \frac{1}{N_n^{1/2}}\int_0^L \psi_n(z)u_g(z,t)dz \tag{34}$$

and the inverse transform is

$$u_g(z,t) = \sum_{n=1}^{\infty} \frac{T_n(t)\psi_n(z)}{N_n^{1/2}} \tag{35}$$

Applying the operator $\frac{1}{N_r^{1/2}}\int_0^L (\cdot)\psi_r(z)dz$ to Eq. (35) can obtain the inverse transform Eq. (34):

$$\frac{1}{N_r^{1/2}}\int_0^L u_g(z,t)\psi_r(z)dz$$
$$= \frac{1}{N_r^{1/2}}\int_0^L \sum_{n=1}^{\infty}\frac{T_n(t)\psi_n(z)}{N_n^{1/2}}\psi_r(z)dz \tag{36}$$
$$= \frac{T_n(t)}{N_r^{1/2}}\sum_{n=1}^{\infty}\int_0^L \frac{\psi_n(z)\psi_r(z)}{N_n^{1/2}}dz = T_n(t)$$

By performing the operator $\int_0^L (\cdot)\psi_r(z)dz$, Eq. (21) can be rewritten as follows:

$$\int_0^L \frac{\partial u_g}{\partial t}\psi_r(z)dz$$
$$= \int_0^L \frac{\theta_g D_s}{\theta_g + H_g\theta_w}\frac{\partial^2 u_g}{\partial z^2}\psi_r(z)dz$$
$$+ \int_0^L \frac{\partial(\theta_g D_s)/\partial z - (v_w H_g + v_g)}{\theta_g + H_g\theta_w}\frac{\partial u_g}{\partial z}\psi_r(z)dz \tag{37}$$
$$- \int_0^L \frac{\partial(v_w H_g + v_g)/\partial z + \mu\theta_g}{\theta_g + H_g\theta_w}u_g\psi_r(z)dz$$
$$+ \int_0^L G\psi_r(z)dz$$

Substituting Eq. (35) into Eq. (37) yields:

$$\frac{dT_n(t)}{dt} + \sum_{r=1}^{\infty}H_{nr}T_r(t) = G_n \quad n = 1,2,...,\infty \tag{38}$$

where

$$H_{nr} = -\frac{1}{N_n^{1/2}N_r^{1/2}}\int_0^L \frac{\theta_g D_s}{\theta_g + H_g\theta_w}\frac{\partial^2\psi_n(z)}{\partial z^2}\psi_r(z)dz$$
$$- \frac{1}{N_n^{1/2}N_r^{1/2}}\int_0^L \frac{\partial(\theta_g D_s)/\partial z - (v_w H_g + v_g)}{\theta_g + H_g\theta_w}\frac{\partial\psi_n(z)}{\partial z}$$
$$\psi_r(z)dz$$
$$+ \frac{1}{N_n^{1/2}N_r^{1/2}}\int_0^L \frac{\partial(v_w H_g + v_g)/\partial z + \mu\theta_g}{\theta_g + H_g\theta_w}\psi_n(z)\psi_r(z)dz \tag{39}$$

$$G_n = \frac{1}{N_n^{1/2}}\int_0^L G(z,t)\psi_r(z)dz \tag{40}$$

The initial condition of Eq. (38) can be obtained by substituting Eq. (25) into Eq. (34) as follows:

$$\left.T_n(t)\right|_{t=0} = \frac{1}{N_n^{1/2}}\int_0^{L_c}$$
$$\psi_n(z)\left[g(z) - (1-z/L)B_t|_{t=0} - C_t z/L\right]dz \tag{41}$$

The analytical solution to Eqs. (38) to (41) can be expressed in matrix form as follows:

$$\mathbf{T}(t) = \exp(-\mathbf{H}t)\mathbf{T}(0) + \int_0^t \exp(-\mathbf{H}(t-\tau))\mathbf{G}d\tau \tag{42}$$

where $\mathbf{T}$ is a vector consisting of $T_n(t)$; $\mathbf{G}$ is a vector consisting of G_n; and $\mathbf{H}$ is a $n \times n$ matrix consisting of elements H_{nr}. The matrix exponential in Eq. (42) can be accurately computed in several different ways, such as Taylor series methods, ordinary differential equation (ODE) methods and polynomial methods [13, 43, 44].

Substituting Eq. (42) into the inverse transform (35) leads to the expression of $u_g(z, t)$ as follows:

$$u_g(z,t) = \mathbf{Y}^T \left[\exp(-\mathbf{H}t)\mathbf{T}(0) + \int_0^t \exp(-\mathbf{H}(t-\tau))\mathbf{G}\mathrm{d}\tau \right] \tag{43}$$

where $\mathbf{Y}$ is a vector consisting of $\frac{\psi_n(z)}{N_n^{1/2}}$.

Data availability The data used to support the findings of this study are available from the corresponding author upon request.

Declarations

Conflict of interest The authors declare that there is no conflict of interest regarding the publication of this paper.

References

1. Andriani D, Atmaja TD (2019) The potentials of landfill gas production: a review on municipal solid waste management in Indonesia. J Mater Cycles Waste Manag 21:1572–1586. https://doi.org/10.1007/s10163-019-00895-5

2. Chattopadhyay AK, Dey PK, Ghosh SK (2017) Dynamics of spatial heterogeneity in a landfill with interacting phase densities–a stochastic analysis. Appl Math Model 41:350–358. https://doi.org/10.1016/j.apm.2016.08.026

3. De Gioannis G, Muntoni A, Cappai G, Milia S (2009) Landfill gas generation after mechanical biological treatment of municipal solid waste Estimation of gas generation rate constants. Waste Manag 29(3):1026–1034. https://doi.org/10.1016/j.wasman.2008.08.016

4. Feng S, Leung AK, Liu HW, Ng CWW, Tan WP (2020) Modelling microbial growth and biomass accumulation during methane oxidation in unsaturated soil. Can Geotech J 57(2):189–204. https://doi.org/10.1139/cgj-2018-0147

5. Feng S, Leung AK, Ng CWW, Liu HW (2017) Theoretical analysis of coupled effects of microbe and root architecture on methane oxidation in vegetated landfill covers. Sci Total Environ 599:1954–1964. https://doi.org/10.1016/j.scitotenv.2017.04.025

6. Feng S, Ng CWW, Leung AK, Liu HW (2017) Numerical modelling of methane oxidation efficiency and coupled water-gas-heat reactive transport in a sloping landfill cover. Waste Manage 68:355–368. https://doi.org/10.1016/j.wasman.2017.04.042

7. Feng SJ, Zhu ZW, Cheng ZL, Chen HX (2020) Analytical model for multicomponent landfill gas migration through four-layer landfill biocover with capillary barrier. Int J Geomech 20(3):04020001. https://doi.org/10.1061/(ASCE)GM.1943-5622.0001598

8. Gardner WR (1958) Some steady-state solutions of the unsaturated moisture flow equation with application to evaporation from a water table. Soil Sci 85(4):228–232. https://doi.org/10.1097/00010694-195804000-00006

9. Gong DY, Shi PJ, Wang JA (2004) Daily precipitation changes in the semi-arid region over northern China. J Arid Environ 59(4):771–784. https://doi.org/10.1016/j.jaridenv.2004.02.006

10. Huang RQ, Wu LZ (2012) Analytical solutions to 1-D horizontal and vertical water infiltration in saturated/unsaturated soils considering time-varying rainfall. Comput Geotech 39:66–72. https://doi.org/10.1016/j.compgeo.2011.08.008

11. Leung AK, Ng CWW (2013) Analyses of groundwater flow and plant evapotranspiration in vegetated soil slope. Can Geotech J 50(12):1204–1218. https://doi.org/10.1139/cgj-2013-014

12. Millington RJ (1959) Gas diffusion in porous media. Science 130(3367):100–102. https://doi.org/10.1063/1.3060771

13. Moler C, van Loan C (2003) Nineteen dubious ways to compute the exponential of a matrix, twenty-five years later. SIAM Rev 45(1):3–49. https://doi.org/10.1137/S00361445024180

14. Molins S, Mayer KU (2007) Coupling between geochemical reactions and multicomponent gas and solute transport in unsaturated media: a reactive transport modeling study. Water Resour Res 43(5):W05435. https://doi.org/10.1029/2006WR005206

15. Moon S, Nam K, Kim JY, Hwan SK, Chung M (2008) Effectiveness of compacted soil liner as a gas barrier layer in the landfill final cover system. Waste Manage 28(10):1909–1914. https://doi.org/10.1016/j.wasman.2007.08.021

16. Mrazovac SM, Milan PR, Vojinovic-Miloradov MB, Tosic BS (2012) Dynamic model of methane-water diffusion. Appl Math Model 36(9):3985–3991. https://doi.org/10.1016/j.apm.2011.11.009

17. Nastev M, Therrien R, Lefebvre R, Gelinas P (2001) Gas production and migration in landfills and geological materials. J Contam Hydrol 52(1–4):187–211. https://doi.org/10.1016/S0169-7722(01)00158-9

18. Ng CWW, Chen ZK, Coo JL, Chen R, Zhou C (2015) Gas breakthrough and emission through unsaturated compacted clay in landfill final cover. Waste Manage 44:155–163. https://doi.org/10.1016/j.wasman.2015.06.042

19. Ng CWW, Coo JL, Chen ZK, Chen R (2016) Water infiltration into a new three-layer landfill cover system. J Environ Eng 142(5):04016007. https://doi.org/10.1061/(ASCE)EE.1943-7870.0001074

20. Ng CWW, Liu J, Chen R (2015) Numerical investigation on gas emission from three landfill soil covers under dry weather conditions. Vadose Zone J. https://doi.org/10.2136/vzj2014.12.0180

21. Ng CWW, Liu HW, Feng S (2015) Analytical solutions for calculating pore-water pressure in an infinite unsaturated slope with different root architectures. Can Geotech J 52(12):1981–1992. https://doi.org/10.1139/cgj-2015-0001

22. Parker JC (1989) Multiphase flow and transport in porous media. Rev Geophys 27(3):311–328. https://doi.org/10.1029/RG027i003p00311

23. Philip JR (1969) Theory of infiltration. Adv Hydrosci 5:215–296. https://doi.org/10.1016/B978-1-4831-9936-8.50010-6

24. Qi CD, Huang J, Wang B, Deng SB, Wang YJ, Yu G (2018) Contaminants of emerging concern in landfill leachate in China: a review. Emerg Contaminants 4(1):1–10. https://doi.org/10.1016/j.emcon.2018.06.001

25. Reid RC, Prausnitz JM, Poling BE (1987) The properties of gases and liquids. McGraw-Hill, New York. https://doi.org/10.1126/science.130.3367.100-a

26. Renou S, Givaudan JG, Poulain S, Dirassouyan F, Moulin P (2008) Landfill leachate treatment: review and opportunity.

J Hazard Mater 150(3):468–493. https://doi.org/10.1016/j.jhazmat.2007.09.077

27. Richards LA (1931) Capillary conduction of liquids through porous mediums. Physics 1(5):318–333. https://doi.org/10.1063/1.1745010

28. Schuetz C, Bogner JE, Chanton JP, Blake D, Morcet M, Kjeldsen P (2003) Comparative oxidation and net emissions of methane and selected non-methane organic compounds in landfill cover soils. Environ Sci Technol 37(22):5150–5158. https://doi.org/10.1021/es034016b

29. Shaikh J, Bordoloi S, Yamsani SK, Sekharan S, Sarmah AK (2019) Long-term hydraulic performance of landfill cover system in extreme humid region: field monitoring and numerical approach. Sci Total Environ 688:409–423. https://doi.org/10.1016/j.scitotenv.2019.06.213

30. Shen SL, Chen YM, Zhan LT, Xie HJ, Bouazza A, He FY, Zuo XR (2018) Methane hotspot localization and visualization at a large-scale Xi'an landfill in China: effective tool for landfill gas management. J Environ Manag 107:47–54. https://doi.org/10.1016/j.jenvman.2018.08.012

31. Townsend TG, Wise WR, Jain P (2005) One-dimensional gas flow model for horizontal gas collection systems at municipal solid waste landfills. J Environ Eng 131(12):1716–1723. https://doi.org/10.1061/(ASCE)0733-9372(2005)131:12(1716)

32. Wen W, Lai YM, You ZM (2020) Numerical modeling of water-heat-vapor-salt transport in unsaturated soil under evaporation. Int J Heat Mass Tran 159:120114

33. Wu LZ, Cheng P, Zhou JT, Li SH (2022) Analytical solution of rainfall infiltration for vegetated slope in unsaturated soils considering hydro-mechanical effects. CATENA 217:106472. https://doi.org/10.1016/j.catena.2022.106472

34. Xie HJ, Wang Q, Bouazza A, Feng SJ (2018) Analytical model for vapour-phase VOCs transport in four-layered landfill composite cover systems. Comput Geotech 101:80–94. https://doi.org/10.1016/j.compgeo.2018.04.021

35. Yu ZG, Leung Y, Chen YD, Chen YQ, Zhang Q, Anh V, Zhou Y (2014) Multifractal analyses of daily rainfall time series in Pearl river basin of China. Physica A 405:193–202. https://doi.org/10.1016/j.physa.2014.02.047

36. Zhan LT, Jia GW, Chen YM, Fredlund DG, Li H (2013) An analytical solution for rainfall infiltration into an unsaturated infinite slope and its application to slope stability analysis. Int J Numer Anal Methods Geomech 37(12):1737–1760. https://doi.org/10.1002/nag.2106

37. Zhan LT, Li GY, Jiao WG, Wu T, Lan JW, Chen YM (2016) Field measurements of water storage capacity in a loess-gravel capillary barrier cover using rainfall simulation tests. Can Geotech J 54(11):1523–1536. https://doi.org/10.1139/cgj-2016-0298

38. Zhan LT, Ng CWW (2004) Analytical analysis of rainfall infiltration mechanism in unsaturated soils. Int J Geomech 4(4):273–284. https://doi.org/10.1061/(ASCE)1532-3641(2004)4:4(273)

39. Zhan LT, Qiu QW, Xu WJ (2016) Analytical solution for infiltration and deep percolation of rainwater into a monolithic cover subjected to different patterns of rainfall. Comput Geotech 77:1–10. https://doi.org/10.1016/j.compgeo.2016.03.008

40. Zhan LT, Qiu QW, Xu WJ, Chen YM (2016) Field measurement of gas permeability of compacted loess used as an earthen final cover for a municipal solid waste landfill. J Zhejiang Univ-Sci A 17(7):541–552. https://doi.org/10.1631/jzus.A1600245

41. Zhan LT, Wu T, Feng S, Li GY, He HJ, Lan JW, Chen YM (2020) Full-scale experimental study of methane emission in a loess-gravel capillary barrier cover under different seasons. Waste Manage 107:54–65. https://doi.org/10.1016/j.wasman.2020.03.026

42. Zhang DF, Wang JD, Chen CL (2020) Gas and liquid permeability in the variably saturated compacted loess used as an earthen final cover material in landfills. Waste Manage 105:49–60. https://doi.org/10.1016/j.wasman.2020.01.030

43. Zhu SR, Wu LZ, Huang J (2022) Application of an improved P(m)-SOR iteration method for flow in partially saturated soils. Computat Geosci 26(1):131–145. https://doi.org/10.1007/s10596-021-10114-6

44. Zhu SR, Wu LZ, Song XL (2022) An improved matrix split-iteration method for analyzing underground water flow. Eng Comput-Germany. https://doi.org/10.1007/s00366-021-01551-z